ELSEVIER

Review

Recent pulsed EPR studies of the Photosystem II oxygen-evolving complex: implications as to water oxidation mechanisms

R. David Britt[a,*], Kristy A. Campbell[a,1], Jeffrey M. Peloquin[a,2], M. Lane Gilchrist[a,3], Constantino P. Aznar[a], Michelle M. Dicus[a], John Robblee[b,4], Johannes Messinger[b,5]

[a] Department of Chemistry, University of California, Davis, 1 Shields Avenue, Davis, CA 95616, USA
[b] Melvin Calvin Laboratory, Physical Biosciences Division, Lawrence Berkeley National Laboratory, and the Department of Chemistry, University of California, Berkeley, CA 94720-5230, USA

Abstract

The pulsed electron paramagnetic resonance (EPR) methods of electron spin echo envelope modulation (ESEEM) and electron spin echo-electron nuclear double resonance (ESE-ENDOR) are used to investigate the structure of the Photosystem II oxygen-evolving complex (OEC), including the paramagnetic manganese cluster and its immediate surroundings. Recent unpublished results from the pulsed EPR laboratory at UC-Davis are discussed, along with aspects of recent publications, with a focus on substrate and cofactor interactions. New data on the proximity of exchangeable deuterons around the Mn cluster poised in the S_0-state are presented and interpreted. These pulsed EPR results are used in an evaluation of several recently proposed mechanisms for PSII water oxidation. We strongly favor mechanistic models where the substrate waters bind within the OEC early in the S-state cycle. Models in which the $O-O$ bond is formed by a nucleophilic attack by a Ca^{2+}-bound water on a strong S_4-state electrophile provide a good match to the pulsed EPR data.
© 2004 Elsevier B.V. All rights reserved.

Keywords: ENDOR; ESEEM; Multiline EPR signal; S_0-state; Substrate water binding

1. Introduction

Jerry Babcock had many diverse and exciting research interests, but throughout his career, he always kept a strong focus on electron paramagnetic resonance (EPR) studies in Photosystem II (PSII). This began in his graduate work with Ken Sauer and was maintained throughout his professorial career at Michigan State. Through this time he introduced many students, postdoctoral researchers, and collaborators to the joys (and sometimes unique challenges) of PSII EPR. Those of us in the field owe Jerry a great debt, not only for his own direct contributions to the field, but also for the many ideas he set forth that have motivated and guided so many of our experiments. His enthusiasm in pursuit of knowledge concerning PSII and the related topics discussed in this issue was relentlessly inspiring.

PSII oxygen evolution occurs through a "Kok cycle" of five "S-state" intermediates, S_0 through S_4, where the subscript represents the number of oxidizing equivalents abstracted from the PSII *oxygen-evolving complex* (OEC) by the photoxidized P680[+] Chl species [1]. The OEC consists of a tetranuclear Mn cluster and its ligation sphere, the redox-active tyrosine Y_Z, and the essential cofactor Ca^{2+} [2–5]. Cl^- depletion affects oxygen evolution, but Cl^- may be playing a secondary role, as opposed to being directly involved in water splitting [6]. As seen in Fig. 1, continuous wave (CW) EPR signals showing degrees of resolved [55]Mn
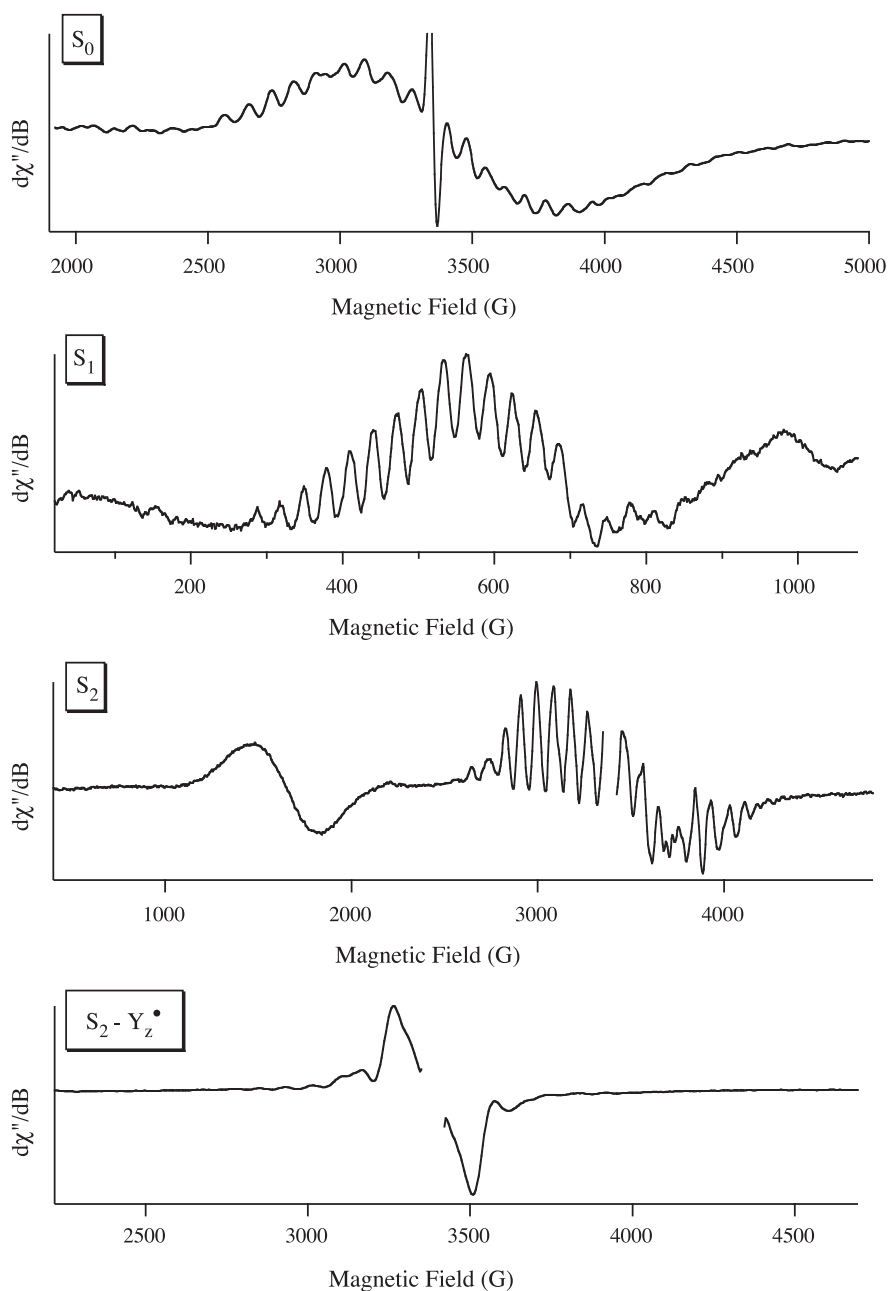
Fig. 1. Several manganese CW-EPR Signals from the PSII OEC, labelled by S-state [7]. Specific preparation and illumination details: The S_0 multiline EPR signal was generated by three flash illumination of spinach thylakoid membranes [10]. The S_1 multiline EPR signal was observed by parallel mode EPR detection of dark-adapted *Synechocystis* PSII particles [32]. The S_2 multiline and $g = 4.1$ EPR signals was generated by 195 K illumination of spinach thylakoid membranes. The S_2-$Y_{\dot{z}}$ EPR signal was generated in acetate inhibited spinach thylakoid membranes frozen during illumination [56].

hyperfine interactions have been assigned to various S-states [7], and their detailed analysis has added much to our current knowledge of the structure, protein ligation, and substrate and inhibitor binding modes of the Mn cluster. However, CW EPR spectroscopy has inherent resolution limitations that can often be overcome by performing pulsed EPR experiments, which can be used to generate detailed structural information concerning paramagnetic metal centers such as the manganese cluster of PSII. Generally, the

use of multi-pulse electron spin echo sequences negates inhomogeneous broadening that tends to dominate EPR line shapes of biological metal centers [7–9]. Specifically, electron spin echo envelope modulation (ESEEM) and electron spin echo-electron nuclear double resonance (ESE-ENDOR) methods can be used to detect nuclear spin transitions of magnetic nuclei close to the manganese cluster of the OEC poised in different S-states. Magnetic nuclei may be naturally present (e.g. ^{55}Mn, ^{1}H, ^{14}N), or may be

introduced through incorporation of labelled amino acids, substrates, inhibitors, or cofactors (e.g. ^{2}H, ^{15}N, ^{13}C, ^{87}Sr).

In this article, we focus on results related to substrate and cofactor binding in the OEC. We introduce new ^{2}H ESEEM results investigating the proximity of exchangeable deuterons around the Mn cluster poised in the S_0-state. As requested by the editors of this special issue dedicated to Jerry Babcock, we also discuss recent unpublished pulsed EPR results, as well as recent publications based on work with the pulsed EPR instrument at UC-Davis. We examine several mechanistic models in the literature, with an emphasis on how well the pulsed EPR data fit with each of these proposed mechanisms.

2. Materials and methods

2.1. Preparation of concentrated S_0/S_1-state samples

PSII samples containing approximately 50% S_0-state and 50% S_1-state were prepared as described previously [10,11] with some modifications outlined below:

PSII membranes were prepared from fresh spinach leaves by a 2 min incubation of the isolated thylakoids with the detergent Triton X-100 [12,13]. The samples were then resuspended to a chlorophyll (Chl) concentration of 6.5 mg Chl/ml in sucrose buffer (pH 6.5, 400 mM sucrose, 50 mM MES, 15 mM NaCl, 5 mM MgCl$_2$, 5 mM CaCl$_2$), frozen as droplets, and stored at -80 °C until used. Chl concentrations were calculated as described in Porra et al. [14].

Before laser flash illumination (800 mJ/pulse at 532 nm, 9 ns pulse width), the PSII membranes were thawed on ice, diluted to a concentration of 1 mg Chl/ml in sucrose buffer, and 3 ml aliquots were transferred in darkness into tissue culture flasks (25 cm^2 growth area). Each sample was illuminated with one pre-flash and dark-adapted for 90 min on ice.

After dark-adaptation, phenyl-1,4-benzoquinone (PPBQ, 50 mM in EtOH) was added to each flask to a final concentration of 100 μM, and then each sample was illuminated with three flashes at a 1 Hz repetition frequency. Immediately after flashing, all samples were combined, and carbonyl cyanide 4-(trifluoromethoxy) phenylhydrazone (FCCP, 5 mM in EtOH) and MeOH were added to final concentrations of 2.5 μM and 1% (v/v), respectively. FCCP accelerates the deactivation of the S_2- and S_3-states of PSII to the S_1-state [15] and reduces Y_D, the stable tyrosine radical of PSII [16]. The latter reaction essentially eliminates the main path for the decay of the S_0-state, which is the oxidation of the S_0-state to the S_1-state by Y_D [17,18]. A small concentration of MeOH is required for the detection of the S_0-state multiline EPR signal [10,19,20]. The samples were collected and centrifuged at 4 °C for 10 min at $48,000 \times g$. The PSII pellets were then resuspended to a concentration of about $10-15$ mg Chl/ml in sucrose buffer

containing 1% MeOH. To allow the conversion of the mixed S_0/S_1-state samples into essentially pure S_1-state samples (see below), dichlorophenyldimethyl urea (DCMU, 100 mM in EtOH) was added to a final concentration of 500 μM. Then the samples were transferred under very dim green light into EPR tubes and concentrated inside the EPR tubes to about $20-30$ mg Chl/ml by centrifugation for 40 min at $6000 \times g$ (4 °C) in a swinging bucket rotor using special adapters. Finally, the supernatants were removed and the samples were frozen in liquid nitrogen. Quantitation of the S_0-state population was performed on parallel samples based on the ratio of the S_2-state multiline EPR signals that can be induced by 200 K illumination in S_0/S_1 samples and S_1 control samples, respectively (for details see Ref. [11]).

^{2}H$_2$O samples were prepared following the same protocol, with the exception that after the first spin the samples were washed once in ^{2}H$_2$O-buffer, centrifuged again at 4 °C for 10 min at $48,000 \times g$, and then resuspended in ^{2}H$_2$O-buffer containing 1% MeOH.

2.2. Turnover of concentrated S_0/S_1-state samples into pure S_1-state samples

In our experience, it is crucial to obtain good S-state difference ESEEM spectra in order to null out contributions from PSII background signals. After taking the ESEEM spectra of the samples poised with significant S_0-state population, the samples were converted to the S_1-state in order to obtain the ESEEM background spectra required for subtraction. This was achieved by quickly thawing the samples, followed by a 2 min continuous illumination with white light and a subsequent 2 min dark-adaptation. All these steps were carried out in a 20 °C water bath. Then the samples were quickly frozen in liquid nitrogen, after which the ESEEM background spectra were obtained. As confirmed by X-band CW EPR spectroscopy (data not shown), centers in the S_0-state are converted by this procedure into the S_1-Q_A^--DCMU state. In contrast, centers in the S_1-state are first oxidized by the illumination to S_2-Q_A^--DCMU, but quickly relax to S_1-Q_A^--DCMU during the subsequent dark adaptation. Therefore, this procedures yields samples with nearly 100% S_1-state population, of which about 50% have reduced Q_A^-.

PSII preparation details related to other pulsed EPR experiments reported in this review are described in the relevant publications, including several manuscripts in preparation.

2.3. Pulsed EPR

ESEEM spectra were collected at a temperature of 4.2 K using a laboratory-built pulsed EPR spectrometer [21]. Three-pulse ESEEM experiments were performed by incrementing the time T in the stimulated echo sequence: $\pi/2-\tau-\pi/2-T-\pi/2-\tau$-stimulated echo. Time domain ESEEM difference spectra were collected as described above for

both ^2H_2O-exchanged and natural abundance water buffer samples. These difference spectra were then each normalized and then ratioed ($^2H_2O/^1H_2O$) to eliminate contributions to the ESEEM modulation from nuclei other than deuterons. A small positive baseline correction was applied to the ratioed time domain data in order to zero the echo trace at times (>2 μs) after the strong deuterium modulation is fully damped. A cosine Fourier backfill was used to reconstruct the dead time data needed to generate the cosine Fourier transform [22]. ESEEM time domain patterns were simulated using a density matrix simulation program [23].

3. Results

3.1. Exchangeable hydrogens

In general, the ESEEM and ENDOR techniques allow one to probe for paramagnetic metal couplings to protons, and to distinguish between sites labile or inert to hydrogen isotope exchange through the introduction of ^2H_2O-enriched buffer, resulting in a loss of a proton signal and a gain of a deuteron signal for exchange-labile sites. Given that the exchange of substrate water as measured by mass spectrom-

Fig. 2. (A) Three-pulse $^2H_2O/^1H_2O$ ratioed time domain ESEEM of the S_2-state (solid line) and a simulation (dotted line). The experimental spectrum shows the ratio of illuminated-minus dark spectra obtained for ^2H_2O-exchanged vs. normal buffer samples. Simulation parameters are included in Table 1. (B) Three-pulse $^2H_2O/^1H_2O$ ratioed time domain ESEEM of cryogenically illuminated (200 K) (trace A) vs. annealed (1 min, 273 K) (trace B)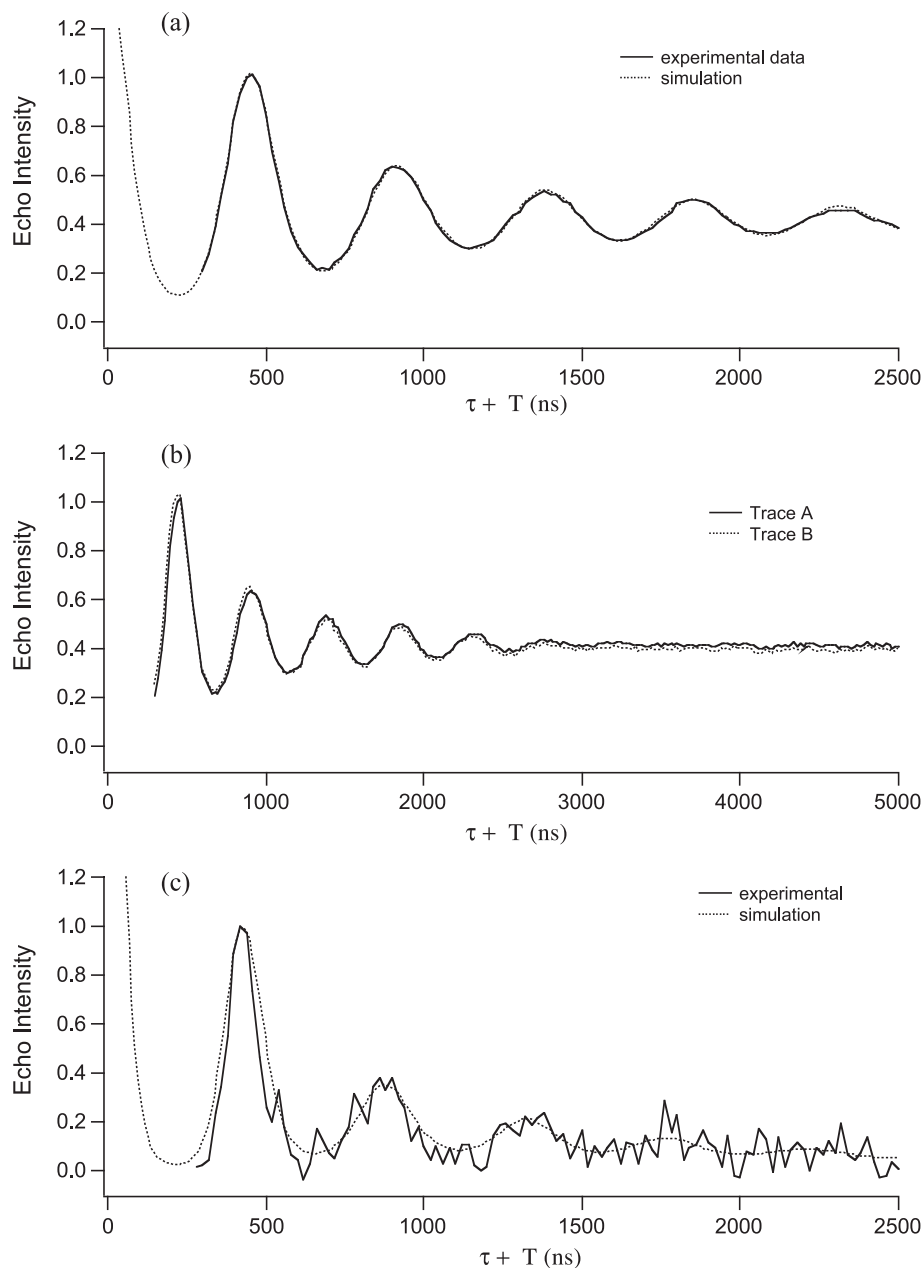. (C) Three-pulse $^2H_2O/^1H_2O$ ratioed time domain ESEEM of the S_0-state (solid line) and a simulation (dotted line). Simulation parameters are included in Table 2.

etry [24–27] is fast on the minutes-to-hours time scale that we are currently using for deuterium exchange with ^2H_2O-enriched buffer, any hydrogen sites of substrate water-derived ligands will be deuterated. In this section, we focus on deuteron ESEEM experiments probing the proximity of exchangeable hydrogens to the manganese cluster in the early steps (S_0–S_2) of the S-state cycle.

3.2. The S_2-state

Fig. 2A shows the three-pulse time domain ESEEM spectrum of the deuterons coupled to the S_2-state Mn cluster following exchange with ^2H_2O-enriched buffer. Specifically, illuminated-minus-dark ESEEM data sets for ^2H_2O-exchanged and normal buffer samples are ratioed ($^2H_2O/^1H_2O$) to isolate the contributions from the exchanged nuclei. The dotted line is a simulation using parameters that also provide good simulations for the two-pulse ESEEM and the corresponding ^1H Davies ESE-ENDOR [28] and ^2H Mims ESE-ENDOR [29] spectra. Experimental and simulation details will be provided elsewhere (Gilchrist et al., manuscript in preparation). A brief discussion of the simulation strategy of ENDOR-constrained ESEEM simulations applied to the S_2-state was recently provided [30].

The S_2-state simulation parameters are shown in Table 1. Four classes of coupled deuterons are employed. One class (A) consists of two deuterons which have a moderately strong isotropic hyperfine coupling (0.45 MHz), as well as a dipolar coupling (0.64 MHz) which in a point-dipole approximation corresponds to a relatively short 2.67 Å distance. A second class (B) consists of two deuterons, with no isotropic coupling, with a short point dipolar distance of 2.71 Å. A third class (C) consists of two deuterons, with no isotropic coupling, with a longer dipolar distance of 3.43 Å. These classes are all manifested in the analogous ^1H ESE-ENDOR spectra and simulations (not shown; Gilchrist et al., manuscript in preparation). Additional "ambient water" shells out to 6 Å represent more distant deuterons. Given that Davies ENDOR is sensitive only to strongly coupled nuclei, these additional weakly coupled hydrogen nuclei are largely suppressed in the corresponding Davies ENDOR spectra. The overall deuteron modulation depth for the S_2-state is quite large. In fact, the deuteron modulation for the

S$_2$-state multiline EPR signal is comparable to what we observe for "bare" Mn(II)aqua ions in ^2H_2O [31], a qualitative indication that numerous exchangeable hydrogens are in contact with the PSII Mn cluster.

3.3. The S_1-state

Unlike the S_2- and S_0-states, the Mn cluster in the dark-stable S_1-state does not present an S = 1/2 perpendicular mode EPR signal. Synechocystis PSII particles show a ^{55}Mn hyperfine rich parallel mode signal [32] (Fig. 1), and potentially this is a target for future parallel mode ESEEM experiments [33]. However, there is another route to gain information about the S_1-state ligation environment. In general, if a cryogenic temperature redox reaction can generate a paramagnetic species at a temperature sufficiently low to "freeze in" the ligation environment of its diamagnetic precursor, this precursor ligand environment can be probed with EPR/ENDOR spectroscopy. Then by raising the temperature in an "annealing" step, the ligand environment can relax to the equilibrium state for the paramagnetic species. Recently, Davydov et al. [34–36] have very fruitfully employed this approach through γ-radiation-induced reduction of heme enzymes. PSII offers the intrinsic advantage that S-state oxidation is generated by visible light. The $S_1 \rightarrow S_2$ state transition can be driven at low temperature (for example, 195 K). Some years ago we demonstrated the use of the annealing method for ESEEM experiments on ammonia binding [23], following CW EPR studies by the Brudvig group [37,38]. For this case, short-term illumination of dark-adapted S_1-state samples at 195 K produced neither the ammonia-altered CW EPR line shape nor ammonia-derived ESEEM features. However, following a 30 s annealing step at 20 °C, ESEEM features attributable to Mn binding of an ammonia (either $^{14}NH_3$ or $^{15}NH_3$) derived ligand appeared along with the associated change in CW EPR line shape. Thus the preferred S_2-state ligation sphere includes the ammonia-derived ligand, but it is unable to bind at the 195 K illumination temperature during the short illumination period (we note that a relatively slow interconversion to the altered EPR form has been found by longer term sample incubation at similar temperatures ($t_{1/2} \approx 15$ min at 198 K) [39]).

We can repeat this experiment with ^1H_2O and ^2H_2O to look for uptake or loss of a water-derived ligand on the $S_1 \rightarrow S_2$ state transition. Fig. 2B shows the ratioed $^2H_2O/^1H_2O$ three-pulse ESEEM time domain spectra for illuminated (195 K, Trace A) and subsequently annealed samples (1 min, 273 K, Trace B) (Gilchrist et al., manuscript in preparation). Some S_2-state multiline signal is lost by charge recombination in the annealing step, so the traces are rescaled to overlap. One sees that the overall shape of the ^2H modulation is essentially the same between illuminated and annealed samples, and therefore the annealing step introduces no appreciable change in the environment of exchangeable

Table 1
Simulation parameters for the S_2-state

	Number of ^2H	A_{iso} (MHz)	A_{dip} (MHz)	r_{eff} (Å)
A	2	0.45	0.64	2.67
B	2	0.00	0.61	2.71
C	2	0.00	0.30	3.43
	ambient waters	0.00	≤ 0.19	≥ 4.0

NQR parameters: $e^2qQ = 0.22$ MHz and $\eta = 0.10$. A_{iso}, A_{dip} and r_{eff} are defined as the isotropic hyperfine coupling constant (Fermi contact), anisotropic hyperfine coupling constant (dipolar coupling) and the effective nucleus–electron distance.

hydrogens around the Mn cluster. We therefore favor very similar exchangeable hydrogen environments for the Mn cluster in the S_1- and S_2-states.

3.4. The S_0-state

In this paper we present new ESEEM data on the proximity of exchangeable hydrogens near the Mn cluster poised in the S_0-state, the initial state of the Kok cycle. These data result from a collaboration between the UC-Davis and UC-Berkeley/Lawrence Berkeley Laboratory groups. Sample preparation details are provided in Materials and methods. Since the S_1-state is dark-stable, generating the S_0-state with illumination requires three flashes to transiently form the S_4-state, followed by a rapid (1 ms) conversion to the S_0-state concomitant with O_2 production and release. The ratioed $^2H_2O/^1H_2O$ three-pulse time domain ESEEM spectrum for the S_0-state is shown in Fig. 2C. This ESEEM pattern shows more noise than the analogous S_2-state data, in part because a smaller fraction of the centers are poised in the S_0-state, and also because of faster electron spin echo dephasing (from two-pulse ESEEM data, not shown). However, it is quite clear that the S_0-state spectrum is very deeply modulated, and therefore the Mn cluster in the S_0-state is readily accessed by deuterons introduced from ^2H_2O.

The S_0-state deuteron modulation is not only very deep, but it also damps out more quickly than the corresponding S_2-state pattern. Fast damping of three-pulse modulation is indicative of strong anisotropic hyperfine couplings, because a broad powder pattern in the frequency domain maps onto a rapidly damped cosine function in the conjugate time domain. The dashed line shows a simulation of the $^2H_2O/^1H_2O$ ratioed S_0-state time domain spectrum. Simulation parameters are included in Table 2. These parameters are not as constrained as the corresponding S_2-state parameters, not only because of lower signal-to-noise for the data, but also because we do not currently have pulsed ENDOR data to tightly constrain the ESEEM simulations. Relative to the S_2-state simulation parameters, we have added another isotropically and dipolar-coupled deuteron (class D) at close distance [40]. The hyperfine parameters for the other classes are varied by modestly small amounts relative to S_2 (note

Table 2
Simulation parameters for the S_0-state

	Number of ^2H	A_{iso} (MHz)	A_{dip} (MHz)	r_{eff} (Å)
A	2	0.40	0.85	2.43
B	2	0.00	0.70	2.59
C	2	0.00	0.40	3.12
D	1	0.30	0.75	2.53
	ambient waters	0.00	≤ 0.19	≥ 4.0

NQR parameters: $e^2qQ = 0.22$ MHz and $\eta = 0.10$. A_{iso}, A_{dip} and r_{eff} are defined as the isotropic hyperfine coupling constant (Fermi contact), anisotropic hyperfine coupling constant (dipolar coupling) and the effective nucleus–electron distance.

the two states of the Mn cluster have different distributions of spin densities, as manifested in the different ^{55}Mn hyperfine patterns of the corresponding CW EPR spectra (Fig. 1)). By no means is this considered a "unique fit" for the S_0-state, but it is certainly suggestive of the intimate accessibility of deuterons from ^2H_2O in this first state of the S-state cycle.

4. Discussion

The experimental result that defines the Kok S-state cycle [1] is the flash dependence of O_2 release. At which point(s) in the cycle the two substrate water molecules bind to the OEC remains an open question. There are 15 possibilities for how the two waters could bind among the five S-states. One limiting case has both waters binding at the S_0-state, presumably to coordination positions opened by the release of O_2 in the $S_4 \rightarrow S_0$ transition. The other limiting case is for the two waters to bind only at S_4, when the OEC is "fully charged" for the water splitting reaction. A possible rationale for this limiting model would be to prevent formation and release of damaging partially oxidized byproducts.

The pulsed EPR experiments such as described in this article allow us to probe for direct water binding as well to address the protonation states of ligands. In addition to the pulsed EPR approach, other techniques such as time resolved mass spectrometry [24–27] and FTIR [41,42] and CW ENDOR [43,44] spectroscopy can provide valuable and complementary evidence regarding the S-state dependence of water binding.

The pulsed EPR data presented in Results clearly show that deuterons from ^2H_2O are introduced into the immediate environment of the Mn cluster at the core of the OEC in the early S-states ($S_0–S_2$). Tables 1 and 2 include both isotropic and dipolar hyperfine contributions. The isotropic coupling is a measure of the delocalization of the unpaired electron wave function, largely centered on the manganese cluster, out onto the specific nucleus. The isotropic interaction is thus a measurement of the covalency of a metal/ligand interaction. A nonzero isotropic coupling and a short dipolar-coupling-estimated distance to deuterons from ^2H_2O is strongly suggestive of direct manganese ligation [45]. Thus from the S_2-state simulations, with two isotropically coupled deuterons, we favor one H_2O or two OH^- ligands to the Mn cluster at the S_2-state. This is in contrast to an earlier CW ENDOR report that the S_2-state is likely "dry" [43].

On the other hand, a deuteron with zero isotropic coupling is unlikely to be associated with a Mn-bound H_2O or OH^- ligand. Distance information can be extracted from the strength of the dipolar coupling. Tables 1 and 2 list "effective" distances (r_{eff}) in a point-dipole approximation. This is only a very rough measure of the true distance however, since for a tetranuclear Mn cluster the effective unpaired spin density is distributed throughout the cluster,

for example as specifically observed for the S_2-state by ^{55}Mn ENDOR [7,46,47]. For a given structural and electronic model for the cluster, contour surfaces of constant dipolar coupling can be generated, and this leads to a better interpretation of distance than the point dipole approximation (vide infra) [45,48].

4.1. Mechanistic implications

From the pulsed EPR data and analysis for states S_0 through S_2 (Fig. 2), we favor models in which the substrate waters enter early in the cycle, perhaps both by the S_0-state, and strongly disfavor models in which the Mn cluster is shielded from water until the last (S_3 or S_4) states. This is certainly consistent with the mass spectrometry results, which indicate that at least one substrate is bound in the OEC in all S-states (see Ref. [27]), and that both waters are bound by the S_2-state [25]. We cannot directly prove with the current data that the pulsed EPR experiments are detecting substrate as opposed to "structural" waters, but it seems unlikely that the highly oxidized Mn cluster,

focussed on controlled, efficient water oxidation, would be ligated by excess water. Therefore our working assumption, consistent with the mass spectrometry results, is that we are indeed probing substrate ligation. There are a number of recent mechanistic proposals that fit within the framework of early S-state water binding. We choose several interesting examples to examine in further detail:

4.1.1. Yachandra et al., 1996

Over the years there have been quite a few models which invoke bridging oxo groups as the source of oxygen in the final dioxygen formation step (e.g. Refs. [49,50]). A recent example of this class of mechanism was provided by Yachandra et al. [4]. In this EXAFS inspired mechanism (Fig. 3a), O_2 is produced via condensation of two bridging oxo's of a high valence Mn dimer (one of two in the dimers-of-dimers model). To fit the short 2.7 Å Mn–Mn distance observed via EXAFS for the S_1- and S_2-states, these oxo bridges must be deprotonated by these steps of the Kok cycle. This would seem inconsistent with our S_2-state pulsed EPR data. As mentioned above, one

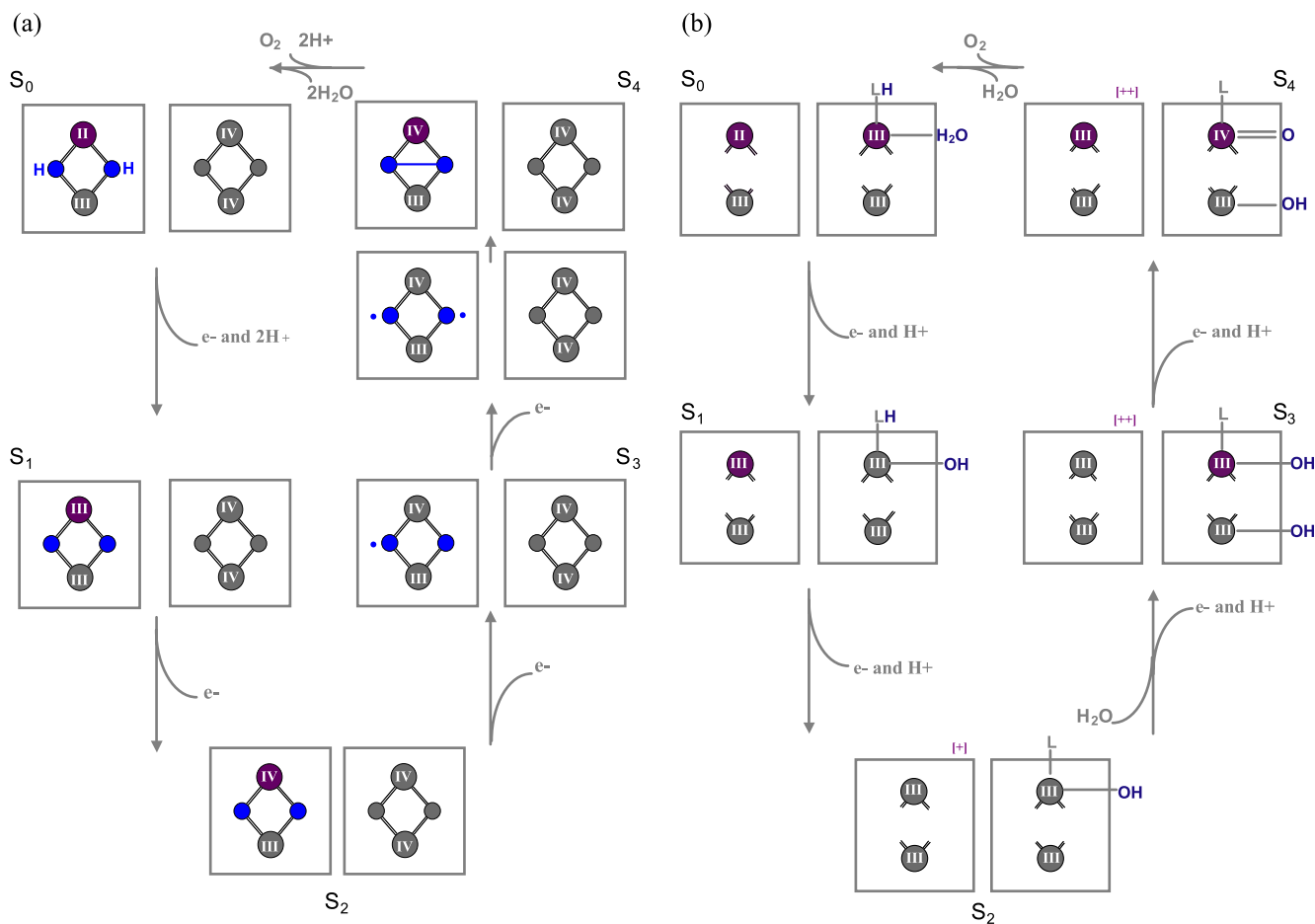Fig. 3. A summary of several proposed water oxidation mechanisms. Water-derived substrate molecules are highlighted in blue. Manganese centered oxidations coupled to S-state transitions are denoted with magenta for the relevant coupled S-states. (a) Yachandra et al. [4]; (b) Hillier and Wydrzynski [27]; (c) Hoganson et al. [51]; (d) Hoganson and Babcock [52]; (e) Vrettos et al. [60].
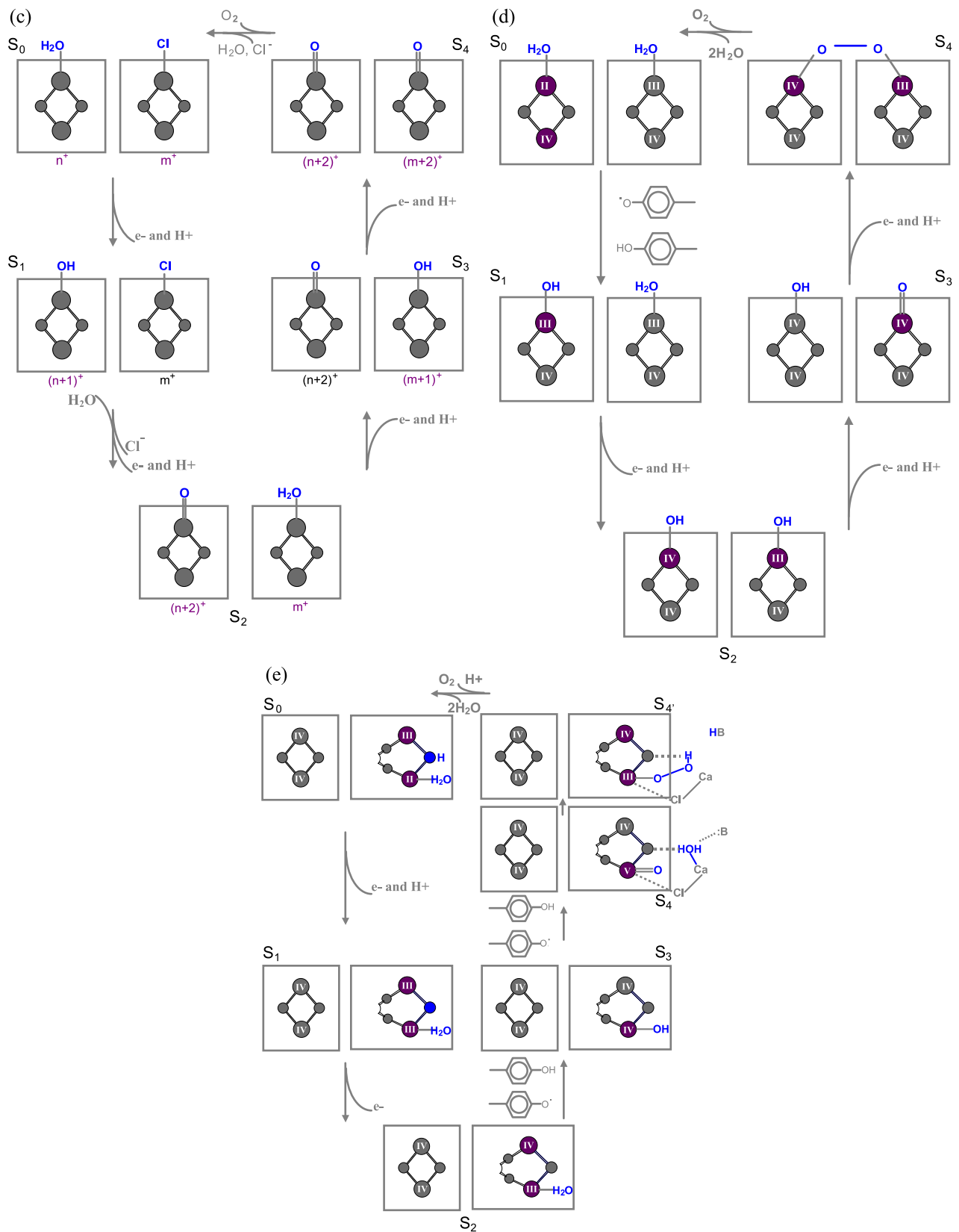
Fig. 3 (*continued*).

caveat to this observation is that it could be argued that the pulsed EPR spectroscopy is observing some sort of structural waters or water-derived ligands, and that the actual substrates are bound in deprotonated bridge sites. However, this seems inconsistent with the aforementioned fast rates for substrate exchange as measured by time-resolved mass spectrometry monitoring the isotopic composition of O_2 evolved from injected $H_2^{18}O$ [24–27].

4.1.2. Hillier and Wydrzynski, 2001

In a review article [27] focussed on oxygen exchange rates, Hillier and Wydrzynski suggest an S-state dependence of substrate ligation to the Mn cluster, including specific oxidation state assignments. These assignments are heavily based on modeling the isotope exchange data. In this proposal (Fig. 3b), one water binds at the S_0-state, but the second water only binds (as an OH^-) at the S_3-state. The S_1- and S_2-state would only have a single Mn(III)-bound OH group, which corresponds to a lower number of isotropically coupled deuterons than our pulsed EPR data suggest.

4.1.3. Hoganson et al., 1995; Hoganson and Babcock, 1997; Tommos and Babcock, 1998

Starting in 1995, Jerry Babcock and associates proposed a radically different mechanism, with the idea that the neutral tyrosine radical $Y_{\dot{Z}}$ abstracts hydrogen atoms from Mn-bound H_2O/OH^- substrate ligands at each Kok cycle transition. This proposal has been very influential. In the first version (Fig. 3c) [51], the authors proposed a Cl^- to H_2O ligand switch upon the $S_1 \rightarrow S_2$-state conversion, coupled to a H-atom abstraction from an OH^- bound to another Mn ion. This proposal would not fit with the lack of change of the ESEEM between the S_1- and S_2-states. In a later paper [52] (also see Ref. [53]), the authors deleted this ligand switch, and the change in ligation upon the $S_1 \rightarrow S_2$-state transition was simply the conversion of a Mn-bound H_2O to an OH^- through H-atom abstraction (Fig. 3d). One could therefore expect a loss of deuteron modulation on the $S_1 \rightarrow S_2$-state transition, but here our illumination vs. annealing approach may not be adequate. It is quite possible that rapid proton or H-atom transfer could occur at the 195 K illumination temperature (as opposed to swapping a whole ligand such as H_2O for Cl^-). However, the recent PSII X-ray structures [54,55] show a relatively long manganese-tyrosine Y_Z distance (approximately 7 Å), consistent with our final analysis of the S_2-$Y_{\dot{Z}}$ interaction EPR (Fig. 1) and ^{55}Mn ENDOR spectra [56]. It is not at all clear whether low temperature H-atom transfer could readily occur over such a long distance, which probably mandates intervening species such as a water bridge (for example as shown in Fig. 14 of Ref. [7]). The H-atom abstraction model proposed by Babcock and associates is highly innovative, and though it remains controversial (see for example Ref. [57]), it has seeded key elements in other mechanistic proposals that invoke $Y_{\dot{Z}}$ in proton-coupled electron transfer (vide infra).

4.1.4. Messinger et al., 1995; Pecoraro et al. 1998; Limburg et al. 1999; Vrettos et al. 2001

Several models for O_2-evolution have been based on an asymmetric binding motif for the two substrate molecules, resulting in a strong electrophile at the S_4-state which is subject to nucleophilic attack by the second substrate. Specifically, Pecoraro et al. [58], Limburg et al. [59], and Vrettos et al. [60] have discussed models in which one substrate water binds to the Mn cluster, but the other binds to the calcium cofactor, with the idea that by the S_4-state, the Mn bound species is highly electron deficient, for example, a Mn(V)=O. This is the electrophile that is subject to nucleophilic attack by the calcium-bound substrate (H_2O or OH^-). Messinger et al. [24] had previously forwarded a similar reactivity model in the context of their oxygen isotope exchange results, which showed one slow and one fast exchange site at the S_3-state. The slowly exchanged S_3-state site was proposed to be a terminal Mn(IV)=O, which would be transiently oxidized in the $S_3 \rightarrow S_4$ transition. The fast exchange site was proposed to be a non-manganese site, with either Ca^{2+} or a protein residue offered as possibilities. More recent ^{18}O exchange experiments [26] employing strontium substitution for calcium have directly implicated calcium in the binding of one substrate water (although in contrast to Ref. [24], it is the slower exchanged site implicated here).

This mechanistic class, with one substrate bound to the Mn cluster and the other to calcium, has a certain appeal from the point of view of our S_2-state pulsed EPR data, in that the simulations reveal two isotropically coupled hydrogen nuclei (Table 1; class A) which could be assigned to the Mn-bound water, along with two hydrogen nuclei with strong dipolar couplings, and therefore short point-dipole distances, but with no isotropic hyperfine interaction (Table 1; class B), which could be assigned to the Ca-bound water. Fig. 4 shows a model for the S_2-state of the OEC based on this idea. Our earlier analysis of the S_2-state ^{55}Mn ENDOR, including the observation that all four Mn ions show significant unpaired spin density, led us to favor a set of tetranuclear Mn cluster models (see Ref. [4] for a number of possible geometries consistent with EXAFS data alone) arranged with a core of three strongly antiferromagnetically coupled Mn ions, with a fourth Mn at a longer distance with a magnetic interaction to the trimer core that is weaker than the intra-trimer couplings [46]. Within the limited resolution, the recent PSII X-ray structures appears to support one such 3 + 1 structure [54,55], and thus we use this structure as a core element of this S_2-state model [61]. This specific Mn cluster geometry is also consistent with recent S_0-state EXAFS results suggestive of three di-μ-oxo bridges in the cluster [11]. Vrettos et al. [60] used a di-manganese analog of oxyhemerythrin as the core element in their reactivity model, and we incorporate this element into the 3 + 1 model as the site formed between the "dangler" Mn and the proximal Mn ion of the trimer core. Calculations of contours of constant dipolar hyperfine field strength are consistent
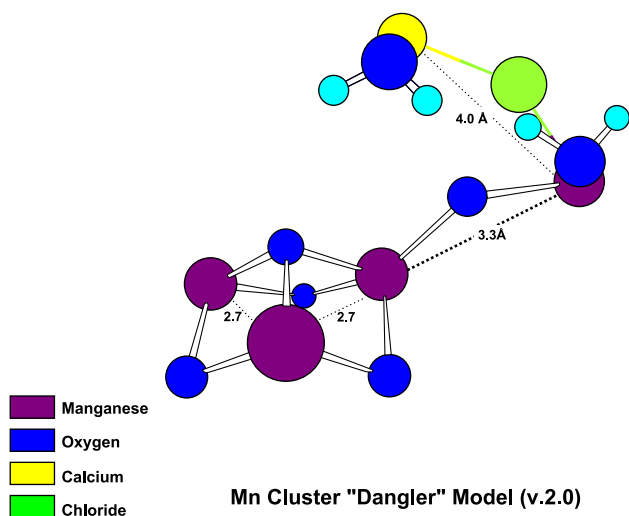
Fig. 4. A model of the S_2-state of the OEC, employing a $3+1$ tetranuclear manganese cluster.

with assigning the two isotropically coupled deuterons (class A) found in the S_2-state simulations to the water bound to the dangler Mn as shown (Gilchrist et al., manuscript in preparation). The strongly and purely dipolar coupled deuterons (class B) appear too close to the Mn cluster to assign to exchangeable hydrogens of Mn ligands such as histidine, aspartate, or glutamate. Such ligand exchangeable sites are more likely to contribute to the "ambient water" component, or possibly to the intermediate distance class C. The class B deuterons are nicely accommodated in the hyperfine contour plots in positions corresponding to the hydrogens of a nucleophilic Ca^{2+}-

bound water (Gilchrist et al., manuscript in preparation), and this is illustrated in Fig. 4.

This S_2-state model also provides a facile match of the lower S-state (S_0-S_2) pulsed EPR data to the specific protonation states and patterns of electron and proton transfer proposed by Vrettos et al. (Fig. 3e). Fig. 5 shows this in detail. The S_2-state is as shown in Fig. 4. The $S_1 \rightarrow S_2$-state transition only involves electron transfer, leaving the protonation state of OEC water-derived ligands the same, as suggested by the pulsed EPR data, and consistent with observed proton release patterns [62]. The $S_0 \rightarrow S_1$-state transition only directly involves electron transfer, but EXAFS analysis has suggested a protonated μ-oxo bridge in the trimer core in the S_0-state [11], and such a proton would be lost upon the oxidation of the cluster to the S_1-state (also see Ref. [60]). Within the context of this model, we assign the additional isotropically coupled deuteron (class D) employed in the S_0-state ESEEM simulation to this protonated (deuterated) OH bridge. Our pulsed EPR data do not extend past the S_2-state, but in Fig. 5 we show $Y_{\dot{Z}}$-driven proton-coupled electron transfers (ala Vrettos et al. [60]) for the remaining two transitions, generating the reactive S_4-state electrophile species (Mn(V)=O or Mn(IV)=O-radical).

4.1.5. Other pulsed EPR data relevant to this model

4.1.5.1. The Ca^{2+}/Sr^{2+} site.
One requirement of this specific model is the proximity of the calcium cofactor, given the central role of the calcium-bound H_2O in nucleophilic attack at the S_4-state. In principle such a nucleophile could correspond to H_2O bound to a lower valence Mn ion, but this would result in additional isotropically coupled hydrogens
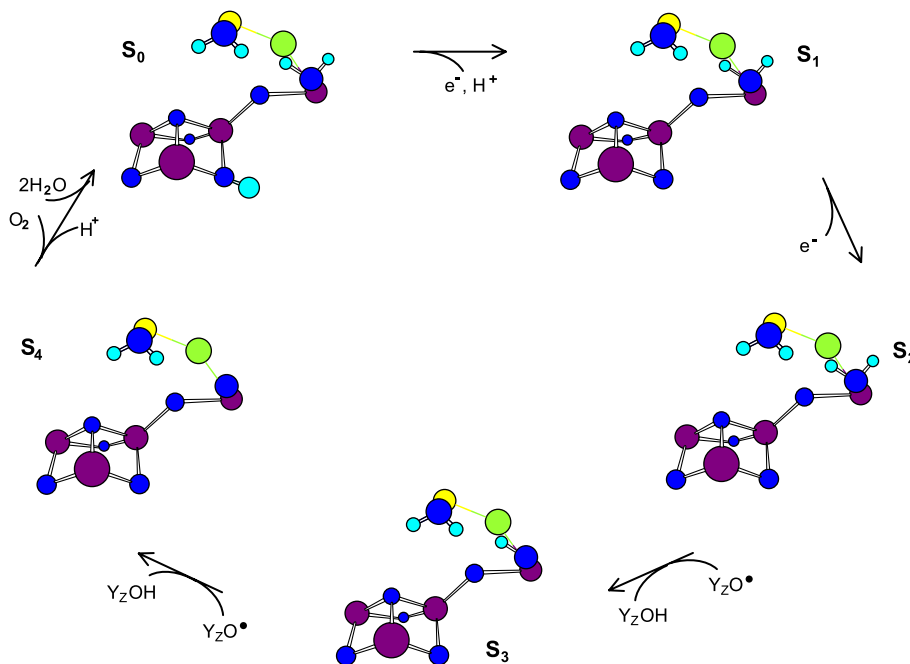

Fig. 5. An S-state model, analogous to Vrettos et al. [60] (Fig. 3e), using a $3+1$ "dangler" motif for the Mn cluster (Fig. 4).

not observed in the pulsed EPR data. As a required cofactor, calcium is clearly important, yet its location is PSII was not identified in the recent X-ray structures [54,55]. There has been debate among EXAFS groups concerning the proximity of calcium to the Mn cluster. Yachandra, Sauer, Klein and co-workers have used Mn, Ca, and Sr EXAFS along with Sr^{2+}-substitution to argue for a close $Mn-Ca^{2+}/Sr^{2+}$ distance, on the order of 3.5 Å [63–65]. In contrast, Riggs-Gelasco et al. report no changes in the Mn EXAFS upon Sr^{2+} or Dy^{3+} substitution for Ca^{2+} [66].

Thus it is timely to introduce another spectroscopic approach to address the possible location of calcium within the environs of the OEC. In principle, ESEEM spectroscopy targeting the magnetic ^{43}Ca nucleus could provide a test, but this 0.135% natural abundance nucleus is prohibitively expensive. Fortunately, strontium, the one metal that functionally substitutes for calcium in the active site of the OEC, has a spin $I = 9/2$ isotope, ^{87}Sr, which is more abundant (7%) and more affordable. Also, Sr^{2+}-substitution for Ca^{2+} gives rise to an altered S_2-state multiline EPR signal [67]. We have used ^{87}Sr-enriched PSII membranes to probe for the proximity of the Ca^{2+}/Sr^{2+} site to the S_2-state Mn cluster (Kim et al., manuscript submitted). We observe ESE modulation at the low ^{87}Sr Larmor frequency (0.6 MHz in our X-band instrument (in contrast to ≈ 15 MHz for ^1H) in the ^{87}Sr data, while this modulation is absent in the natural abundance Sr data. A simulation of the ^{87}Sr data fits (within the limited signal-to-noise of this low γ nucleus) with a $Mn-^{87}Sr$ point-dipolar distance of 4.5 Å. As for the hydrogen nuclei, the point dipolar distance is only a rough measure of the true distance, which will depend on the orientation of the various Mn-nucleus vectors with respect to the cluster and its distributed spin density. The salient point is that these results provide an independent new spectroscopic result for the close proximity of the Ca^{2+}/Sr^{2+} site to the Mn cluster, which is a necessary condition for the calcium-nucleophile model.

A possible objection to this calcium-nucleophile model is the relatively slow ^{18}O isotope exchange rate for the calcium/strontium-substitution sensitive substrate site over the S-states measured [26]. This is many orders of magnitude slower than the solution exchange rate for Ca^{2+} in water [24,27]. The presence of diffusion bottlenecks introduced by the protein may slow the diffusion rate, but it is not clear that this is sufficient to slow the exchange by seven to eight orders of magnitude. Strong hydrogen-bonding, for example to the adjacent $Mn-O-Mn$ bridge, could further slow exchange. An endpoint view could be to have the Ca^{2+}-bound water/hydroxide bridge back to the Mn cluster [26], but in this picture we lose the appealing assignment of the close class B hydrogen with no isotropic coupling. However, we certainly cannot rule out the formation of such a bridge after the S_2-state, for example in the $S_2 \rightarrow S_3$ transition.

4.1.5.2. Ammonia and alcohol binding. We have previously used ESEEM to examine ammonia [23] and alcohol

[48] binding in proximity to the Mn cluster in the S_2-state. Based on the quantitative nature of ESEEM simulations, we concluded that one ammonia binds at the S_2-state in the ammonia-treated samples. Likewise, in PSII membranes with full extrinsic polypeptide composition, one methanol is bound at the S_2-state. We have recently examined whether ammonia and methanol can bind simultaneously at the S_2-state by titrating these two water analogs in samples where deuterated methanol was used as an ^2H ESEEM target (Evanchik et al., manuscript in preparation). This study concludes that both ammonia and methanol bind in non-competitive sites at the S_2-state. Given that both ammonia and methanol could bind as water analogs, it is appealing to postulate that these substitute for the two substrate waters in the doubly treated samples. Of interest is the fact that at the S_2-state, one ammonia-derived ligand is bound and one methanol is bound, as opposed to, for example, two ammonia-derived or two methanol ligands. This supports the idea that asymmetric binding environments are present at the S_2-state, consistent with the Mn cluster and Ca^{2+} binding sites of Fig. 4.

As described earlier, ammonia binds to an ESEEM observable site only on the $S_1 \rightarrow S_2$-state transition. We favor direct ligation to Mn based on the strength of the isotropic hyperfine interaction, and more specifically, we favor a bridging geometry (for example an NH_2 bridge between Mn ions) based on the large asymmetry of the ^{14}N electric quadrupolar interaction [23]. The Mn oxidation in the $S_1 \rightarrow S_2$-state transition may be required to trigger the NH_3 deprotonation required to form this bridge. For ESEEM experiments done in ^2H_2O-enriched buffer, in which the added NH_3/NH_4^+ is rapidly equilibrated with the deuteration level of the buffer, there is minimal change in ^2H modulation depth upon ammonia binding (Gilchrist et al., manuscript in preparation), suggesting that the proposed NH_2 bridge substitutes for a Mn-bound water. Such a binding geometry, consistent with the S_2-state model of Fig. 4, is shown in Fig. 6 (top panel). If ammonia bound as a terminal NH_3, one would expect an increase in ^2H ESEEM modulation even if a water were displaced, since two strongly coupled deuterons would be replaced by three. We consider this supporting evidence for the bridging NH_2 hypothesis, which is controversial due to the high solution pK_a of NH_3. On the other hand, if a NH_2 bridge simply replaced a structural oxo bridge [39] without the loss of a water ligand, one would expect a large increase in ^2H ESEEM modulation due to the presence of two additional strongly coupled deuterons. The deuterated ammonia ESEEM data could also be modeled by proposing that two Mn-bound hydroxides are displaced by the bridging NH_2 as opposed to one water. However, the S_2-state pulsed EPR data are adequately modeled by equivalent isotropically and dipolar coupled hydrogen nuclei, which are modeled well by the water-binding geometry in Figs. 4 and 6. On the other hand, one criticism of this geometry, at least in the explicit mechanistic proposal of Vrettos et al., is that the suggested $Mn(III)-OH_2$ to $Mn(IV)-OH$ change upon the
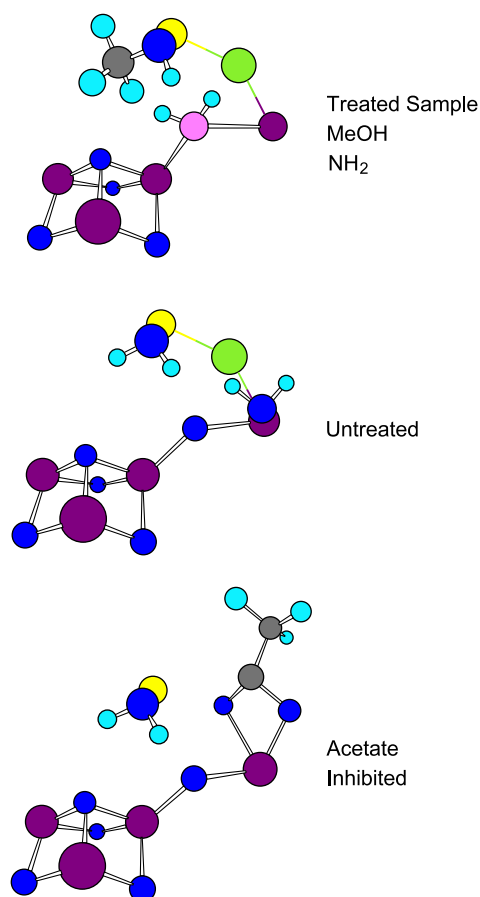
Fig. 6. S_2-state models for the OEC of: (top) ammonia and methanol treated, (center) untreated, and (bottom) acetate-treated PSII samples.

$S_2 \rightarrow S_3$ transition would likely lead to a change in the slow phase oxygen isotope exchange rate, which is not observed in the time-resolved mass spectrometry data [27].

In contrast to the ammonia-treated samples, illuminated vs. annealing experiments of the type previously described, but using methyl-deuterated methanol, show no changes upon annealing, indicating that methanol is bound in an identical environment near the Mn cluster in both S_1- and S_2-states [48]. Good ESEEM simulations can be generated using only dipolar hyperfine couplings, and therefore we have no direct evidence (i.e. isotropic hyperfine couplings) that these alcohols bind directly as ligands to the Mn cluster. Comparing ESEEM experiments done in ^2H_2O-enriched buffer with and without methanol (the MeOH alcohol hydrogen is then deuterated to the extent of the buffer), there is a modest decrease in ^2H modulation depth observed with the alcohol treatment (Gilchrist et al., manuscript in preparation). Within the structural model of Fig. 4, we can postulate that the ESEEM-observed alcohol binds to the calcium substrate site, resulting in a slight decrease in ^2H modulation as two exchangeable hydrogens of H_2O are replaced by one exchangeable hydrogen of MeOH. This motif is also included in Fig. 6 (top panel), which can be compared to the center panel for contrasting the modeled

ammonia/methanol bound S_2-state to the untreated S_2-state (center panel). We note that the link between the ESEEM detecting alcohol binding site discussed here and the well-known effect of alcohols on CW EPR intensities is not so clear: for example isopropanol triggers a $g = 4.1 \rightarrow$ multiline EPR signal conversion at concentrations that do not elicit appreciable isopropanol binding at the ESEEM-detected site in extrinsic-intact PSII membranes [48].

4.1.5.3. Acetate binding. We recently published an ^2H ESEEM study employing methyl-deuterated acetate as a probe for whether this inhibitor binds at the Mn cluster [68]. The ratioed (deuterated acetate/natural abundance acetate) three-pulse ESEEM spectrum shows clear ^2H modulation, and the modulation depth was found to be consistent with direct Mn ligation by acetate. Acetate is considered to be a competitive inhibitor for the Cl^- binding site (e.g. Ref. [69]), so this is suggestive of chloride ligation to the Mn cluster in the S_2-state. Of particular interest is the result obtained for natural abundance acetate binding in ^2H_2O-enriched buffer, which shows a large decrease in ^2H modulation upon acetate binding. This was modeled in terms of a displacement of two isotropically coupled deuterons. In the context of the structural model of Fig. 4, this would correspond to a loss of the terminal water ligand on the "dangler" Mn ion, as shown in Fig. 6 (bottom panel). In order to include the preferred Cl^- competition, we show a bidentate acetate also displacing Cl^- (although note that Ref. [6] questions a direct cofactor role for Cl^-). Such a bidentate acetate binding geometry is consistent with our analysis of the deuterated acetate ESEEM data [68]. If proton-coupled electron transfer is required to drive the $S_2 \rightarrow S_3$-state transition ([60], Fig. 5), then a dehydration of the Mn water binding site would lead to a Kok cycle lesion between the S_2- and S_3-states, as observed by the formation of the S_2-$Y_Z^\cdot$ split EPR signal in acetate-treated PSII preparations (Fig. 1) [7,56].

5. Conclusions

Pulsed EPR results described examining the proximity of exchangeable hydrogens to the Mn cluster in the lower S-states lead us to strongly favor mechanistic models where the substrate waters bind within the OEC early in the S-state cycle. These magnetic resonance results complement and reinforce recent ^{18}O exchange studies [24–27].

At this time, our pulsed EPR data are limited to the lower S-states (S_0–S_2). But at least through this early window into the oxygen production cycle, mechanistic models in which the O–O bond is formed by a nucleophilic attack by a Ca^{2+}-bound water on a strong S_4-state electrophile provide for facile interpretation of these pulsed EPR data, as well as other data addressing the proximity of the Ca^{2+}/Sr^{2+} cofactor and binding of ammonia, small alcohols, and acetate.

Acknowledgements

References

[1] B. Kok, B. Forbush, M. McGloin, Cooperation of charges in photosynthetic O_2 evolution: I. A linear four step mechanism, Photochem. Photobiol. 11 (1970) 457–475.

[2] R.J. Debus, The manganese and calcium ions of photosynthetic oxygen evolution, Biochim. Biophys. Acta 1102 (1992) 269–352.

[3] R.D. Britt, Oxygen evolution, in: D.R. Ort, C.F. Yocum (Eds.), Oxygenic Photosynthesis: The Light Reactions, Kluwer Academic Publishing, Dordrecht, The Netherlands, 1996, pp. 137–164.

[4] V.K. Yachandra, K. Sauer, M.P. Klein, Manganese cluster in photosynthesis: where plants oxidize water to dioxygen, Chem. Rev. 96 (1996) 2927–2950.

[5] J. Messinger, Towards understanding the chemistry of photosynthetic oxygen evolution: dynamic structural changes, redox states and substrate water binding of the Mn cluster in photosystem II, Biochim. Biophys. Acta 1459 (2000) 481–488.

[6] K. Olesen, L.-E. Andreasson, The function of the chloride ion in photosynthetic oxygen evolution, Biochemistry 42 (2003) 2025–2035.

[7] R.D. Britt, J.M. Peloquin, K.A. Campbell, Pulsed and parallel polarization EPR characterization of the manganese cluster of the photosystem II oxygen evolving complex, Annu. Rev. Biophys. Biomol. Struct. 29 (2000) 463–495.

[8] B.M. Hoffman, V.J. DeRose, P.E. Doan, R.J. Gurbiel, A.L.P. Houseman, J. Telser, Metalloenzyme active-site structure and function through multifrequency cw and pulsed ENDOR, in: L.J. Reuben, J. Reuben (Eds.), Biological Magnetic Resonance, vol. 13. Plenum, New York, 1993, pp. 151–218.

[9] R.D. Britt, Electron spin echo methods: a tutorial, in: J. Telser (Ed.), Paramagnetic Resonance of Metallobiomolecules, ACS Symposium Series, (2003) 16–54.

[10] J. Messinger, J.H. Robblee, W.O. Yu, K. Sauer, V.K. Yachandra, M.P. Klein, The S_0 state of the oxygen-evolving complex in photosystem II is paramagnetic: detection of an EPR multiline signal, J. Am. Chem. Soc. 119 (1997) 11349–11350.

[11] J.H. Robblee, J. Messinger, R.M. Cinco, K.L. McFarlane, C. Fernandez, S.A. Pizarro, K. Sauer, V.K. Yachandra, The Mn cluster in the S_0 state of the oxygen-evolving complex of photosystem II studied by EXAFS spectroscopy: are there three di-oxo-bridged Mn^2 moieties in the tetranuclear Mn complex? J. Am. Chem. Soc. 123 (2002) 7804–7820.

[12] D.A. Berthold, G.T. Babcock, C.F. Yocum, A highly resolved, oxygen-evolving photosystem II preparation from spinach thylakoid membranes, FEBS Lett. 134 (1981) 231–234.

[13] T. Kuwabara, N. Murata, Inactivation of photosynthetic oxygen evolution and concomitant release of three polypeptides in the photosystem II particles of spinach chloroplasts, Plant Cell Physiol. 23 (1982) 533–539.

[14] R.J. Porra, W.A. Thompson, P.E. Kriedemann, Determination of accurate extinction coefficients and simultaneous equations for assaying chlorophyll-a and chlorophyll-B extracted with 4 different solvents—verification of the concentration of chlorophyll standards by atomic absorption spectroscopy, Biochim. Biophys. Acta 975 (1989) 384–394.

[15] B. Hanssum, G. Dohnt, G. Renger, On the mechanism of ADRY agent interaction with the photosystem II donor side, Biochim. Biophys. Acta 806 (1985) 210–220.

[16] G.T. Babcock, K. Sauer, Electron-paramagnetic resonance signal-II in spinach chloroplasts: 2. Alternative spectral forms and inhibitor effects on kinetics of signal-II in flashing light, Biochim. Biophys. Acta 325 (1973) 483–503.

[17] S. Styring, A.W. Rutherford, In the oxygen-evolving complex of photosystem II the S_0 state is oxidized to the S_1 state by Y_D^+ (signal II slow), Biochemistry 26 (1987) 2401–2405.

[18] J. Messinger, W.P. Schröder, G. Renger, Structure–function relations in photosystem II. Effects of temperature and chaotropic agents on the period four oscillation of flash-induced oxygen evolution, Biochemistry 32 (1993) 7658–7668.

[19] J. Messinger, J.H.A. Nugent, M.C.W. Evans, Detection of an EPR multiline signal for the S0* state in photosystem II, Biochemistry 36 (1997) 11055–11060.

[20] K.A. Åhrling, S. Peterson, S. Styring, An oscillating manganese electron paramagnetic resonance signal from the S_0-state of the oxygen evolving complex in photosystem II, Biochemistry 36 (1997) 13148–13152.

[21] B.E. Sturgeon, R.D. Britt, Design of a sensitive pulsed EPR spectrometer with an 8 to 18 GHz frequency range, Rev. Sci. Instrum. 63 (1992) 2187–2192.

[22] W.B. Mims, Elimination of the dead-time artifact in electron spin-echo envelope spectra, J. Magn. Reson. 59 (1984) 291–306.

[23] R.D. Britt, J.-L. Zimmermann, K. Sauer, M.P. Klein, Ammonia binds to the catalytic manganese of the oxygen-evolving complex of Photosystem II. Evidence by electron spin-echo envelope modulation spectroscopy, J. Am. Chem. Soc. 111 (1989) 3522–3532.

[24] J. Messinger, M. Badger, T. Wydrzynski, Detection of one slowly exchanging substrate water molecule in the S_3-state of photosystem-II, Proc. Natl. Acad. Sci. U. S. A. 92 (1995) 3209–3213.

[25] G. Hendry, T. Wydrzynski, The two substrate–water molecules are already bound to the oxygen evolving complex in the S_2-state of photosystem II, Biochemistry 41 (2002) 13328–13334.

[26] G. Hendry, T. Wydrzynski, ^{18}O isotope exchange measurements reveal that calcium is involved in the binding of one substrate–water molecule to the oxygen-evolving complex in photosystem II, Biochemistry 42 (2003) 6209–6217.

[27] W. Hillier, T. Wydrzynski, Oxygen ligand exchange at metal sites—implications for the O_2 evolving mechanism of photosystem II, Biochim. Biophys. Acta 1503 (2001) 197–209.

[28] E.R. Davies, A new pulse ENDOR technique, Phys. Lett. 47A (1974) 1–2.

[29] W.B. Mims, Pulsed ENDOR experiments, Proc.-Roy. Soc. Lond. 283 (1965) 452–457.

[30] C.P. Aznar, R.D. Britt, Simulations of the ^1H ESE-ENDOR and ^2H ESEEM spectra of exchangeable hydrogen nuclei coupled to the S_2-state photosystem II manganese cluster, Philos. Trans. R. Soc. Lond., B 357 (2002) 1359–1366.

[31] C.G. Hoogstraten, R.D. Britt, Water counting: quantitating the hydration level of paramagnetic metal ions bound to nucleotides and nucleic acids, RNA 8 (2002) 252–260.

[32] K.A. Campbell, J.M. Peloquin, D.P. Pham, R.J. Debus, R.D. Britt, Parallel polarization EPR detection of an S_1-state "multiline" EPR signal in photosystem II particles from S*ynechocystis* sp. PCC 6803, J. Am. Chem. Soc. 120 (1998) 447–448.

[33] B.E. Sturgeon, P.E. Doan, K.E. Liu, D. Burdi, W.H. Tong, J.M. Nocek, N. Gupta, J. Stubbe, D.M. Kurtz, S.J. Lippard, B.M. Hoffman, Non-Kramers ESEEM of integer-spin diferrous carboxylate-bridged clusters in proteins, J. Am. Chem. Soc. 119 (1997) 375–386.

[34] R. Davydov, B.M. Hoffman, A.M. Valentine, S.J. Lippard, S.G. Sligar,

M. Ikeda-Saito, EPR and ENDOR studies on cryoreduced metalloproteins, J. Inorg. Biochem. 74 (1999) 110.

[35] R. Davydov, T.M. Makris, V. Kofman, D.E. Werst, S.G. Sligar, B.M. Hoffman, Hydroxylation of camphor by reduced oxy-cytochrome p450cam: mechanistic implications of EPR and ENDOR studies of catalytic intermediates in native and mutant enzymes, J. Am. Chem. Soc. 123 (2001) 1403–1415.

[36] R. Davydov, V. Kofman, H. Fujii, T. Yoshida, M. Ikeda-Saito, B.M. Hoffman, Catalytic mechanism of heme oxygenase through EPR and ENDOR of cryoreduced oxy-heme oxygenase and its Asp 140 mutants, J. Am. Chem. Soc. 124 (2002) 1798–1808.

[37] W.F. Beck, G.W. Brudvig, Binding of amines to the O_2-evolving center of photosystem II, Biochemistry 25 (1986) 6749–6756.

[38] W.F. Beck, J.C. de Paula, G.W. Brudvig, Ammonia binds to the manganese site of the O_2-evolving complex of Photosystem II in the S_2 state, J. Am. Chem. Soc. 108 (1986) 4018–4022.

[39] A. Boussac, A.W. Rutherford, S. Styring, Interaction of ammonia with the water splitting enzyme of photosystem II, Biochemistry 29 (1990) 24–32.

[40] We note that with the noise level of the data a third isotropically coupled deuteron added to "class A" rather than into a new "class D" also gives an acceptable simulation.

[41] T. Noguchi, M. Sugiura, FTIR detection of water reactions during the flash-induced S-state cycle of the photosynthetic water-oxidizing complex, Biochemistry 41 (2002) 15706–15712.

[42] T. Noguchi, M. Sugiura, Structure of an active water molecule in the water-oxidizing complex of photosystem II as studied by FTIR spectroscopy Noguchi, Biochemistry 39 (2000) 10943–10949.

[43] X.S. Tang, M. Sivaraja, G.C. Dismukes, Protein and substrate coordination to the manganese cluster in the photosynthetic water oxidizing complex: ^{15}N and ^1H ENDOR spectroscopy of the S_2 state multiline signal in the thermophilic cyanobacterium S*ynechococcus elongatus*, J. Am. Chem. Soc. 115 (1993) 2382–2389.

[44] R. Fiege, W. Zweygart, R. Bittl, N. Adir, G. Renger, W. Lubitz, EPR and ENDOR studies of the water oxidizing complex of photosystem II, Photosynth. Res. 48 (1996) 227–237.

[45] D.W. Randall, A. Gelasco, V.L. Pecoraro, R.D. Britt, ESE-ENDOR and ESEEM characterization of water and methanol ligation to a dinuclear Mn(III)Mn(IV) complex, J. Am. Chem. Soc. 119 (1997) 4481–4491.

[46] J.M. Peloquin, K.A. Campbell, D.W. Randall, M.A. Evanchik, V.L. Pecoraro, W.H. Armstrong, R.D. Britt, ^{55}Mn ENDOR of the S_2-state multiline EPR signal of photosystem II: implications on the structure of the tetranuclear Mn cluster, J. Am. Chem. Soc. 122 (2000) 10926–10942.

[47] J.M. Peloquin, R.D. Britt, EPR/ENDOR Characterization of the physical and electronic structure of the OEC Mn cluster, Biochim. Biophys. Acta 1503 (2001) 96–111.

[48] D.A. Force, D.W. Randall, G.A. Lorigan, K.L. Clemens, R.D. Britt, ESEEM studies of alcohol binding to the manganese cluster of the oxygen evolving complex of photosystem II, J. Am. Chem. Soc. 120 (1998) 13321–13333.

[49] G.W. Brudvig, R.H. Crabtree, Mechanism for photosynthetic O_2 evolution, Proc. Natl. Acad. Sci. U. S. A. 83 (1986) 4586–4588.

[50] G. Christou, J.B. Vincent, The molecular 'double-pivot' mechanism for water oxidation, Biochim. Biophys. Acta 895 (1987) 259–274.

[51] C.W. Hoganson, N. Lydakis-Simantiris, X.S. Tang, C. Tommos, K. Warncke, G.T. Babcock, B.A. Diner, J. McCracken, S. Styring, A hydrogen-atom abstraction model for the function of Y_Z in photosynthetic oxygen-evolution, Photosynth. Res. 46 (1995) 177–184.

[52] C.W. Hoganson, G.T. Babcock, A metalloradical mechanism for the generation of oxygen from water in photosynthesis, Science 277 (1997) 1953–1956.

[53] C. Tommos, G.T. Babcock, Oxygen production in nature: a light-driven metalloradical enzyme process, Acc. Chem. Res. 31 (1998) 18–25.

[54] A. Zouni, H. Witt, J. Kern, P. Fromme, N. Krauss, W. Saenger, P.

Orth, Crystal structure of photosystem II from S*ynechococcus elongatus* at 3.8 angstrom resolution, Nature 409 (2001) 739–743.

[55] N. Kamiya, J.R. Shen, Crystal structure of oxygen-evolving photosystem II from *Thermosynechococcus vulcanus* at 3.7 Å resolution, Proc. Natl. Acad. Sci. U. S. A. 100 (2003) 98–103.

[56] J.M. Peloquin, K.A. Campbell, R.D. Britt, ^{55}Mn pulsed ENDOR demonstrates that the photosystem II "split" EPR signal arises from a magnetically-coupled mangano-tyrosyl complex, J. Am. Chem. Soc. 120 (1998) 6840–6841.

[57] R. Ahlbrink, M. Haumann, D. Cherepanov, O. Bogershausen, A. Mulkidjanian, W. Junge, Function of tyrosine Z in water oxidation by photosystem II: electrostatical promotor instead of hydrogen abstractor, Biochemistry 37 (1998) 1131–1142.

[58] V.L. Pecoraro, M.J. Baldwin, M.T. Caudle, W. Hsieh, N.A. Law, A proposal for water oxidation in photosystem II, Pure Appl. Chem. 70 (1998) 925–929.

[59] J. Limburg, V.A. Szalai, G.W. Brudvig, A mechanistic and structural model for the formation and reactivity of a Mn-V=O species in photosynthetic water oxidation, J. Chem. Soc., Dalton Trans. 1999 (1999) 1353–1361.

[60] J.S. Vrettos, J. Limburg, G.W. Brudvig, Mechanism of photosynthetic water oxidation: combining biophysical studies of photosystem II with inorganic model chemistry, Biochim. Biophys. Acta 1503 (2001) 229–245.

[61] In our ^{55}Mn ENDOR paper [44] we pointed out that this "triangle + 1" core structure, one of a set of three $3 + 1$ structures selected from the EXAFS-based models [4], was fully compatible with the EPR/ENDOR analysis. We provided an S_2-state OEC model in this paper (also see Ref. [7]) with a "C-shaped" linearly coupled model to make a minimal change from the "dimers of -dimers" model which had been effectively employed in the Babcock H-atom abstraction mechanism. The "triangle + 1" is magnetically equivalent in its S = 1/2 ground state as long as the three exchange couplings of the core are not equivalent, for example, one no stronger than 1/2 the value of the other two. The current X-ray structural data more resembles the triangle + 1 structure, so we use this in the model of Fig. 4.

[62] E. Schlodder, H.T. Witt, Stoichiometry of proton release from the catalytic center in photosynthetic water oxidation—reexamination by a glass electrode study at pH 5.5–7.2, J. Biol. Chem. 274 (1999) 30387–30392.

[63] M.J. Latimer, V.J. Derose, I. Mukerji, V.K. Yachandra, K. Sauer, M.P. Klein, Evidence for the proximity of calcium to the manganese cluster of photosystem II—determination by X-ray-absorption spectroscopy, Biochemistry 34 (1995) 10898–10909.

[64] R.M. Cinco, J.H. Robblee, A. Rompel, C. Fernandez, V.K. Yachandra, K. Sauer, M.P. Klein, Strontium EXAFS reveals the proximity of calcium to the manganese cluster of oxygen evolving photosystem II, J. Phys. Chem., B 102 (1998) 8248–8256.

[65] R.M. Cinco, K.L. McFarlane Holman, J.H. Robblee, J. Yano, S.A. Pizarro, E. Bellacchio, K. Sauer, V.K. Yachandra, Calcium EXAFS establishes the Mn–Ca cluster in the oxygen-evolving complex of photosystem II, Biochemistry 41 (2002) 12928–12933.

[66] P.J. Riggs-Gelasco, R. Mei, D.F. Ghanotakis, C.F. Yocum, J.E. Penner-Hahn, X-ray absorption spectroscopy of calcium-substituted derivatives of the oxygen-evolving complex of photosystem II, J. Am. Chem. Soc. 118 (1996) 2400–2410.

[67] A. Boussac, A.W. Rutherford, Nature of the inhibition of the oxygen-evolving enzyme of Photosystem II induced by NaCl washing and reversed by the addition of Ca^{2+} or Sr^{2+}, Biochemistry 27 (1988) 3476–3483.

[68] K.L. Clemens, D.A. Force, R.D. Britt, Acetate binding at the photosystem II oxygen evolving complex: an S_2-state multiline signal ESEEM study, J. Am. Chem. Soc. 124 (2002) 10921–10933.

[69] K.V. Kühne, V.A. Szalai, G.W. Brudvig, Competitive binding of acetate and chloride in photosystem II, Biochemistry 38 (1999) 6604–6613.